# Generalized Nighttime Radiative Deficits

John C. Howell, Tomer Yizhaq, Nadav Drechsler, Yuval Zamir, Daniel Beysens, Joseph A. Shaw

Howell, J. C., Yizhaq, T., Drechsler, N., Zamir, Y., Beysens, D., & Shaw, J. A. (2021). Generalized nighttime radiative deficits. Journal of Hydrology, 603, 126971.

# Generalized Nighttime Radiative Deficits

John C. Howell,[1] Tomer Yizhaq,[1] Nadav Drechsler,[1]
Yuval Zamir,[1] Daniel Beysens,[2,3] and Joseph A. Shaw[4]

[1]*Racah Institute of Physics, The Hebrew University of Jerusalem, Jerusalem, Israel, 91904*

[2]*Physique et Mecanique des Milieux Heterogneses,*
*CNRS, ESPCI, PSL Research University,*
*Sorbonne Universite, Sorbonne Paris Cite,*
*10 rue Vauquelin, 75005 Paris, France*

[3]*OPUR, 2 rue Verderet, 75016 Paris, France*

[4]*Electrical and Computer Engineering Dept.,*
*Montana State University, Bozeman, MT 59717*

(Dated: September 8, 2021)

We derive a general, tilt-dependent, nighttime, radiative deficit model with an eye towards improved dew collection. The model incorporates atmospheric/environmental incoming radiation, a linear precipitable water vapor transmittance function dependent on local meteo data and the influence of near-horizon obstacles. A brief discussion of cloud cover is given. The model is then used more specifically to predict radiative deficits for an ideal blackbody emitter in an environment with an isotropic temperature. Knowing the tilt angle, near-horizon obstacles and local meteo-data, it is then possible to estimate the radiative deficit of a given emitter. We consider errors resulting from the assumption that the ground and obstacles are at the same temperature as the air. We also analyze the errors arising from the linear precipitable water vapor transmittance function by comparing the results against high-resolution, full-spectrum Modtran® data [1]. We show that for typical tilt angles, the isotropic temperature model is a reasonable approximation as long as the above-horizon environmental heating is small. We believe these results will be broadly valuable for the field of radiative cooling where a general radiative treatment has yet to be made and in particular the field of dew water harvesting.

## I. INTRODUCTION

While remaining a niche method within the water production landscape, passive dew collection has the distinct advantage of being local, renewable, easy to use, producing relatively clean water and not requiring electricity[2–4]. While dew collection will not solve the world's water problems [5, 6], it can provide an important supplemental source in places where the right atmospheric conditions exist. Between gaseous, liquid and solid phases, there is approximately the equivalent of 12,900 $km^3$ of liquid water in the atmosphere making it a prime source for exploration [7].

Dew was unsuccessfully pursued as a water source in the early 20th century [8]. However, there has been recent renewed interest in dew as a supplemental water source [3, 9–13] as our understanding of condenser physics [8], radiative cooling [14–21], and dew formation [22, 23] have improved, and high-yield materials have come to bear [24–32]. In an effort to optimize dew yields, many parameters have been studied including: wind speed [33, 34], angle of the collector [24, 35], shape of the apparatus [36–40] and scaling of dew collectors [41, 42] to name a few.

The enabling physical mechanism of passive dew collection is radiative cooling [14–21, 27, 43–45]. The atmosphere has a spectral transmission window in the long-wave infrared region roughly between 8 and 13 microns through which the Earth and bodies of similar temperature can undergo thermal exchange with space (treated as an infinite thermal reservoir at 2.7K). A radiative deficit of a device is the cooling that comes from the differential between the blackbody radiated heat loss of the device and the blackbody atmospheric and environmental radiative heat gain back on to the device. If the deficit is large enough and care has been taken to limit other heating sources, the device can cool below the dew point and dew condenses on the surface.

While radiative cooling and dew theory are both fairly mature fields, there have been historical difficulties in linking them together. Optimal radiative deficits and optimal dew collection have competing demands and operate under different contexts. Ideal radiative cooling occurs with the emitter surface normal pointed at the zenith and with low path-integrated precipitable water vapor (PWV). PWV is defined as the liquid equivalent thickness of the water vapor column from the Earth's surface to the top of the atmosphere. On the other hand, to overcome pinning forces of dew droplets on the emitters, it is neces-

sary to tilt the emitter relative to the zenith, which decreases the cooling power. Further, high relative humidity, needed for high dew yields, can also imply high PWV, which lowers the atmospheric transmission and thus reduces the radiative deficit. Although radiative cooling is usually derived using an angularly-dependent sky emissivity, due to these above difficulties, in many dew theory models atmospheric heating is often described by a single, angle-independent, empirical, sky-emissivity parameter $\varepsilon_{atm}$ [3, 8, 46]. Owing to the dynamic nature of the atmosphere, this requires constant surveillance of the atmosphere. Here, we derive a radiative model that incorporates PWV for an angle-dependent emissivity for emitters of arbitrary geometry, but focus on planar emitters tilted at arbitrary angles. The model further considers the effects from near-horizon obstacles as well as cloud cover.

We note that the field of radiative cooling lacks a generalized radiative treatment. The theory and most proof-of-concept emitter deficits are based on surface normals pointing at or near the zenith. However, as the need for radiative cooling increases and, for example paints, are used at non-zenith angles, a generalized treatement will be needed. By adding to this work the direct and indirect solar irradiance (Rayleigh scattered) contributions as well as the emitter absorbance properties in the visible and short wave infrared, a fully generalized treatment could be made.

This paper is organized as follows. We first express the basis for nighttime radiative deficit for tilted emitters. Then we briefly describe the use of a popular atmospheric emissivity model. Next, we consider the effects of the tilt of a perfect blackbody emitter on the radiative deficit in an environment at the temperature of the air. Then, we incorporate a precipitable water vapor model into the atmospheric emissivity. Lastly, we discuss the results and potential errors in the assumptions in a Discussion section.

## II. NIGHTTIME RADIATIVE DEFICITS FOR TILTED EMITTERS

The nighttime radiative deficit (excluding solar heating) of an emitter at temperature $T$ is expressed by the equation:

$$P_{deficit} = P_{rad} - P_{in}, \tag{1}$$

where $P_{rad}$ represents the thermal power radiated from the emitter. For an arbitrary emitter geometry, it is found by integrating the emitted thermal radiation of the dew condenser at temperature $T$ for each infinitessimal area $\boldsymbol{dA}$ of the emitter over all wavelengths $\lambda$ and solid angles $\boldsymbol{d\Omega}$:

$$P_{rad} = \int_A \int_\Omega \boldsymbol{dA} \cdot \boldsymbol{d\Omega} \int_0^\infty I_{BB}(\lambda, T)\varepsilon(\lambda, \theta, \phi)d\lambda, \tag{2}$$

where $I_{BB}$ is the ideal blackbody spectral radiance, and $\varepsilon$ is the emissivity of the emitter, which is a function of polar and azimuthal emission angles and wavelength. From this point, we will assume a planar emitter with unit surface area having a surface normal vector $\boldsymbol{n_e}$, which simplifies our radiated power to

$$p_{rad} = \int \boldsymbol{n_e} \cdot \boldsymbol{d\Omega} \int_0^\infty I_{BB}(\lambda, T)\varepsilon(\lambda, \theta, \phi)d\lambda, \tag{3}$$

where we note that the use of the lower case $p_{rad}$ is the power per unit area.

$P_{in}$ is the thermal downwelling radiation absorbed by the emitter from the atmosphere and environment. In typical radiative cooling theory models, only the atmospheric radiation is assumed. In this calculation, we consider all incoming thermal radiation that impinges on the emitter whether it be from the atmosphere or external objects in the environs that may not have azimuthal symmetry. Also using the power per unit area, we have

$$p_{in} = \int \boldsymbol{n_e} \cdot \boldsymbol{d\Omega} \int_0^\infty I_{BB}(\lambda, T_{env})\varepsilon(\lambda, \theta, \phi)\varepsilon_{env}(\lambda, \theta, \phi, W, c)d\lambda \tag{4}$$

where $\varepsilon_{env}$ is the emissivity of the surrounding environment as a function of polar $\theta$ and azimuthal $\phi$ angles, wavelength $\lambda$ precipitable water vapor (PWV, which in mathmetical expressions is $W$, for simplicity) and cloud cover $c$. We will show how to find $W$ later as a function of air temperature and relative humidity.

In standard solutions for radiative theory, a planar emitter has a surface normal that points at the zenith, $\boldsymbol{n_e} = \hat{\boldsymbol{k}}$, from which we define our polar angle. The azimuthally invariant symmetry of such an emitter is valuable since the atmospheric radiation is also assumed to be azimuthally invariant. Thus, for this symmetric configuration, we find $\boldsymbol{n_e} \cdot \boldsymbol{d\Omega} = \cos(\theta)\sin(\theta)d\theta d\phi$ as described in most radiative theory works.

We now consider a more generalized case of an emitter that is tilted relative to the zenith. We assume that the emitter is rotated about the x-axis by an angle $\theta_e$ such that

$$\boldsymbol{n_e} \cdot \boldsymbol{d\Omega} = [\sin(\theta)\sin(\phi)\sin(\theta_e) + \cos(\theta)\cos(\theta_e)]\sin(\theta)d\theta d\phi \tag{5}$$

$$= f(\theta_e, \theta, \phi)d\theta d\phi \tag{6}$$

which reduces to the standard form in the limit of $\theta_e = 0$.

Equations 1, 3 and 4 are generalized forms of the radiative deficit, emitted and incoming radiation, respectively for a planar emitter. If, for example, the temperature of the atmosphere, temperature of all surrounding objects, the wavelength- and angle-dependent emitter, environmental and sky emissivity (including cloud distributions and temperatures) are known, we can solve these equations directly. However, in many circumstances, only a limited amount of meteo data are available such as the air temperature and relative humidity near the ground. In these circumstances, we can often make several simplifying assumptions without significantly changing the theoretical predictions.

## III. EMISSIVITY MODEL

We break up the environmental emissivity parameter $\varepsilon_{env}$ into two main regions. For the solid angle of the emitter that is concerned with the downwelling radiation from the atmosphere we say that $\varepsilon_{env} = \varepsilon_{atm}$. For simplicity, for all other solid angles, we will assume that the environmental emissivity is unity (an ideal blackbody). While there are numerous mathematical models to describe angle-dependent atmospheric emissivity [47], a simple and popular [2, 18] model of the atmospheric emissivity that incorporates cloud cover is given by

$$\varepsilon_{atm}(\lambda, \theta, W, c) = 1 - (1 - c)t(\lambda, W)^{1/\cos(\theta)} \tag{7}$$

where $t(\lambda, W)$ is the transmission of the atmosphere at the zenith as a function of wavelength, $c$ is the cloud cover which can vary between clear sky with $c = 0$ and completely covered with $c = 1$ and the PWV which can be estimated from the surface temperature and relative humidity. We can see that this emissivity model is an ideal blackbody minus the polar angle-dependent transmissivity. The angular dependence is a purely geometric term that accounts for the atmospheric thickness. We note that this cloud cover model is a time-averaged result with the assumption that the clouds are equally likely to be at any position in the sky.

We further note that this description of cloud cover is overly simplistic. Clouds can have a vast range of temperatures (-80 °C to 30 °C) dependent on height and opacity [48]. In the calculations that follow, we use the clear sky results $c = 0$.

## IV. PERFECT BLACKBODY IN AN ENVIRONMENT OF ISOTROPIC TEMPERATURE

We now seek to solve the radiative deficit under the assumption that a planar emitter is a perfect blackbody, $\varepsilon(\lambda, \theta, \phi) = 1$, in an environment where the temperature is isotropic (the same in all directions relative to the emitter). With this assumption, Eq. 3 reduces to $\sigma T^4$, where $\sigma$ is the Stefan-Boltzmann constant.

Eq. 4 is somewhat complicated. A general solution requires considering four integration regions, two to represent the atmospheric radiation and two to represent the non-atmospheric environmental radiation. The integration regions are shown in Fig. 1. There are four geometric surfaces of importance: the emitter plane, the zenith plane, the horizon plane and an obstacle cone. For the obstacle cone, we make the assumption that the non-atmospheric environment is a uniform temperature blackbody that extends an angle $\alpha$ above the horizon or with polar angle $\pi/2 - \alpha$. Any radiation coming from the environment at a polar angle greater than that defined by the obstacle plane is considered to be from a perfect blackbody. Any flux beyond the azimuthal and polar angles set by the emitter plane produces no net radiative flux and is therefore not integrated. We can simplify our analysis by using the assumptions that the environment and the air are the same temperature and the environment is a perfect blackbody, namely

$$p_{in} = \sigma T_{env}^4 - \int_0^\infty [A_1(\lambda, W, \theta_e, \alpha) + A_2(\lambda, W, \theta_e, \alpha)] I_{BB}(\lambda, T_{env}) d\lambda, \tag{8}$$

where

$$A_1(\lambda, W, \theta_e, \alpha) = \int_0^\pi \int_0^{\pi/2-\alpha} f(\theta_e, \theta, \phi) t(\lambda, W)^{1/\cos(\theta)} d\theta d\phi \tag{9}$$

and

$$A_2(\lambda, W, \theta_e, \alpha) = \int_0^\pi \int_0^{\theta_b(\theta_e, \alpha, \phi)} f(\theta_e, \theta, \phi) t(\lambda, W)^{1/\cos(\theta)} d\theta d\phi \tag{10}$$

represent the differential radiation terms due to the atmospheric transmission window. The

polar integration bound $\theta_b(\theta_e, \phi)$ on $B_2$ is given by

$$\theta_b(\theta_e, \alpha, \phi) = \begin{cases} -\pi/2 + \alpha, \text{ if } \alpha \geq \tan^{-1}(\tan(\theta_e)\sin(\phi)) \\ -\pi/2 + \tan^{-1}(\tan(\theta_e)\sin(\phi)), \text{ otherwise.} \end{cases} \tag{11}$$

Essentially, we have considered the entire solid angle of incoming flux to be from a perfect blackbody and subtracted off the component of the solid angle of the atmosphere where this is not the case. The integration bound $\theta_b(\theta_e, \alpha, \phi)$ defines the region set, either by the emitter plane geometry or the obstacle cone. During the integration process, $\theta_b(\theta_e, \alpha, \phi)$ may switch between the two cases as the azimuthal angle is varied.

One common measure of the radiative cooling power of a given system is the radiative deficit of the emitter at ambient temperature. A widely-used technique for finding the radiative deficit is to place a heater of known power on the side not facing the sky to maintain the ambient temperature of the emitter to compensate the radiative deficit [28]. Under the assumptions then that the emitter, atmosphere and non-atmospheric environment are all the same temperature, the radiative deficit can then be written as

$$p_{deficit}^{ambient} = \int_0^\infty d\lambda [A_1(\lambda, W, \theta_e, \alpha) + A_2(\lambda, W, \theta_e, \alpha)] I_{BB}(\lambda, T_{env}). \tag{12}$$

We will use this ambient-temperature standard throughout the paper. Once we know how $t$ varies with relative humidity and temperature, we can then solve these integrals numerically. We develop a model to do this in the next section.

## V. ATMOSPHERIC TRANSMISSION VS PRECIPITABLE WATER VAPOR

While water vapor is only a trace gas in the atmosphere, it has enormously significant effects on infrared atmospheric transmittance. In fact, the atmospheric transmittance in the region covering a wavelength range of approximately 8-13 $\mu$m is determined primarily by the water vapor content (and secondarily by the $CO_2$ content) [15]. For determining radiative deficits, it is sufficient to know the real-time path-integrated zenith PWV to determine atmospheric transmission. PWV varies from place to place and in time. In situations where it is difficult to know either local or real-time PWV, we can make approximations based on exponential density vapor models if one knows the approximate local atmospheric water

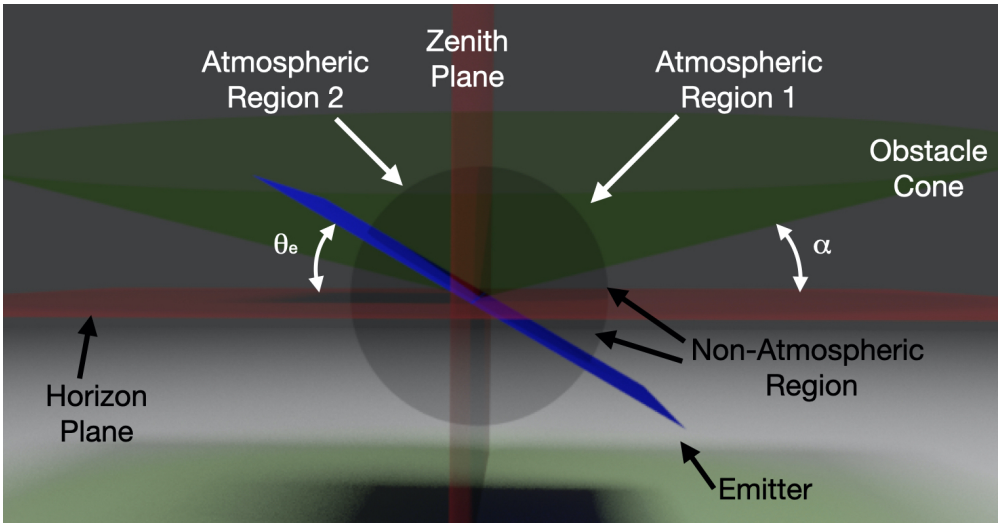


FIG. 1. 3D model of the integration regions for an emitter.

vapor scale height.

The effects of PWV on radiative cooling were first discussed by Bliss [15]. He considered infinite atmospheric slabs of same-pressure and same-temperature water vapor and $CO_2$ and their radiative effects on a horizontal plate. PWV's importance in radiative cooling is well known [15, 43–45]. For example, an empirical and local PWV model based on relative humidity and temperature is described in [45], but that model can only be used in Boulder Colorado. Here we take a general approach. We follow a few step process. First, we calculate the saturation water vapor pressure $P_s$ as a function of temperature $T$ using Teten's equation

$$P_s(T) = 610.78 * \exp\left(\frac{17.27T}{T + 237.3}\right) \tag{13}$$

where $T$ is in Celsius and $P_s$ is in Pascal. We then calculate the saturation vapor density $\rho_s$ from the ideal gas law

$$\rho_s = \frac{P_s M}{R(T + 273.15)}, \tag{14}$$

where $R$, in MKS units, is the universal gas constant, $M = 18.01528$ g/mol is the molar mass of water, resulting in units of $\rho_s$ in g/m$^3$. The vapor density at a given relative humidity is then given by

$$\rho_0 = RH * \rho_s. \tag{15}$$

To a reasonable approximation, the atmospheric water vapor, as measured by its density,

falls off exponentially with height given by

$$\rho(h) = \rho_0 \exp(-h/h_{SC}) \tag{16}$$

where $h_{SC}$ is the atmospheric water vapor scale height parameter in units of kilometers. The precipitable water vapor can then be found from integrating over the water vapor column height

$$W = \frac{10\rho_0}{\rho_{lw}} \int_0^\infty \exp(-h/h_{SC}) dh, \tag{17}$$

where $\rho_{lw}$ is the density of liquid water (1 g per cm$^3$) and $W$ is in units of centimeters (integrating from zero produces PWV from sea level, which should be adjusted for the height of the emitter). For an emitter at sea level, we arrive at the particularly simple solution of

$$W = \frac{10\rho_0}{\rho_{lw}} h_{SC}. \tag{18}$$

We describe a method for determining the local scale height using AERONET data and local meteo data in the Discussion section of the paper. Knowing $W$, one can then use this value to determine the atmospheric transmittance using the Modtran® atmospheric radiative transfer code [1]. We use the Mid-Latitude Summer model that predicts the zenith atmospheric transmittance for a given $W$ (this is a standard option within the Modtran code for simulating typical midlatitude vertical profiles of atmospheric temperature, humidity, pressure, and trace gases [49]). After comparing radiative deficits from Modtran® data, we found that integrating between 8 and 13.5 microns with a Mid-Latitude Summer atmospheric transmittance of

$$t_{ML} = \frac{-0.108}{cm} W + 0.873, \tag{19}$$

where $t_{ML}$ is a unitless quantity and the coefficient in front of $W$ in the equation is in inverse centimeters, gave reasonable agreement with the full Modtran® data-derived results. The use of a simple linear transmittance function such as Eq. 19 not only dramatically reduces computational overhead, but it does away with the need to download new transmission data sets for each PWV (i.e., each unique value of $W$).

With this background, we are now able to solve for the radiative deficit versus emitter tilt and local meteo data. Consider the ambient-temperature radiative deficit predictions shown in Fig. 2 subfigure (a). In this subfigure we have used the linear PWV model described

above to make predictions of the radiative deficit as a function of tilt for an emitter at 15C. The errors in the radiative deficits from using the linear model relative to the full Modtran® transmittance data calculation are shown in subfigure (b). As can be seen, the linear model is a good approximation over a wide range of PWV. The linear PWV model parameters were chosen to minimize errors between 0° and 30° over a range of PWV. The errors in subfigure (b) may come somewhat as surprise in their behavior. This is a result of the highly nonlinear behavior of the atmospheric emissivity (see Eq. 7) and the fact that the transmission function can vary dramatically between between 8 and 13 microns (see Fig. 5).

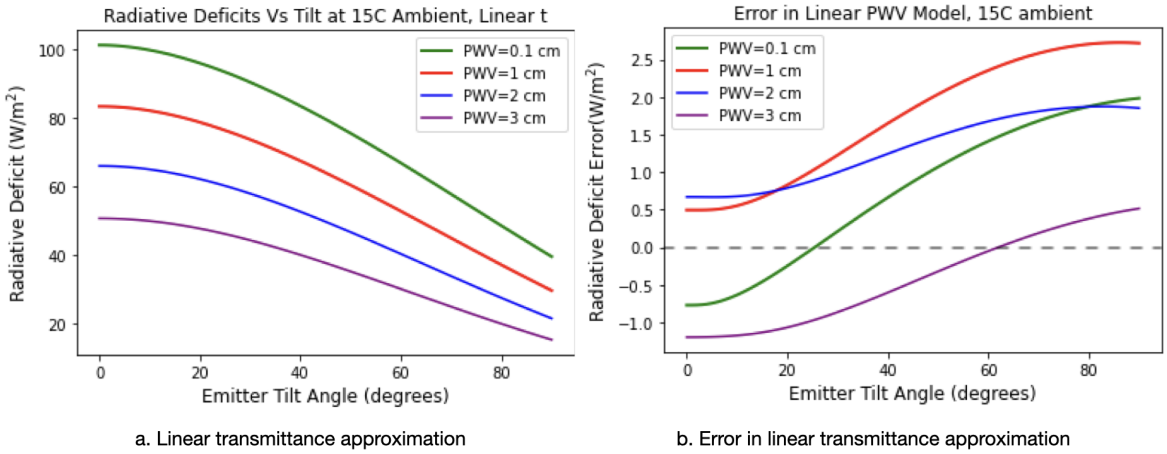


FIG. 2. Predicted ambient-temperature radiative deficits vs emitter tilt angle using (a) linear approximation of the transmittance for various PWV and the obstacle view angle of $\alpha$ = 0. In (b) the errors in the linear model against a full Modtran® data calculation are shown. These calculated powers assume that the emitter is at ambient temperature of 15 °C.

Now we consider the effects of having obstacles above the horizon plane. We make the simplifying assumptions that all obstacles arise above the horizon to the same angle $\alpha$, are all the same temperature as the air, and are continuously uniformly distributed across the horizon. Fig. 3 shows the predicted ambient-temperature radiative deficits for a fixed PWV of 2 cm and ambient temperature of 15° as $\alpha$ takes various values using the linear PWV model. One can see that the difference in the radiative deficit between 0° and 15° is quite small. This is due to the fact that there is much more path-integrated water along the horizon making it practically opaque (nearly an ideal blackbody) to the infrared. However, the cone angle becomes increasingly important.

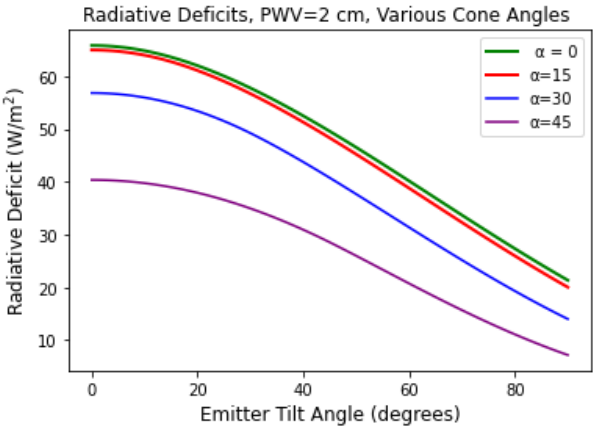


FIG. 3. Predictions of the radiative deficits accounting for obstacles of varying view angle $\alpha$ above the horizon. $\alpha$ is varied between 0 and 45° in increments of 15° assuming a PWV of 2 cm. The radiative deficit is shown for varying the angle of the emitter between 0 and 90°. The linear PWV model was used for these calculations for an ambient temperature of 15°.

## VI. DISCUSSION

Unlike other gases in the atmosphere, the water vapor scale height is location-dependent. For example, the tropics have very large scale heights. The implication then is that while there may be high relative humidity needed for dew condensation, the atmosphere is more opaque to the longwave IR making radiative cooling less effective. The geography surrounding the Mediterranean, for example, tends to have small scale heights, meaning there can be both high relative humidity and low PWV, making it a prime region for performing dew water harvesting.

PWV measurements are collected by over 600 AERONET stations around the world. However, AERONET stations don't measure temperature and humidity. Therefore a weather station close to an AERONET station is needed to determine the local scale height for PWV. Excluding drastic changes in geography, it is reasonable to assume that the scale height is roughly constant at locations within several tens of kilometers. Further, the variations in scale height tend to be much stronger North-South than East-West as can be seen in a global PWV map (e.g., such as is shown in Fig. 4, same altitude different integrated PWV).

The calculations shown here all assumed cloud-free skies ($\boldsymbol{c}$=0). If this assumption were relaxed to account for the presence of clouds, the result would be an increase in atmospheric

emissivity and a corresponding reduction of Earth-space radiation [48]. Eqn. 7 provides a simple method of accounting for this, using the cloud cover factor $\boldsymbol{c}$ that varies from 0 (clear) to 1 (overcast). This simple model treats all clouds as blackbodies that uniformly and perfectly prevent Earth-space radiative transfer. A more complete treatment would account for spatial distributions of cloudiness and variable cloud emissivity. For example, a low-level liquid cloud at the zenith would have a much larger effect than a high-level ice cloud near the horizon. This is because the liquid cloud has a much higher radiative temperature and blocks the otherwise most effective Earth-space radiation path at the zenith, while the ice cloud has a lower radiative temperature and only blocks the near-horizon path where atmospheric transmission is already low (as indicated by the cosine factor in 7).

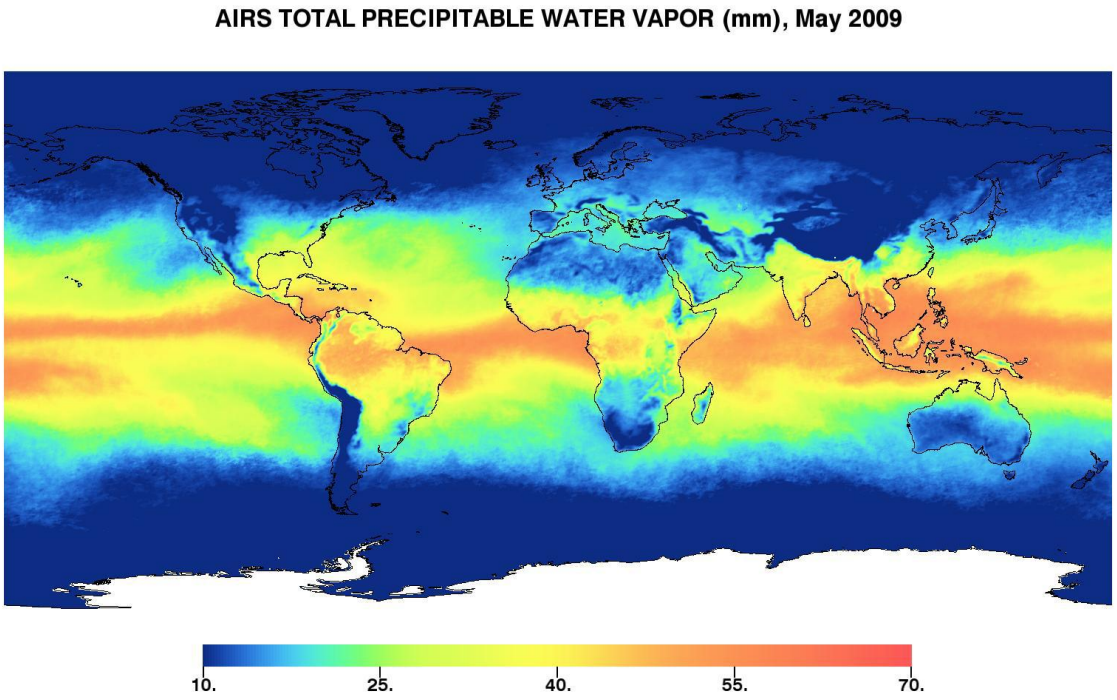


FIG. 4. Global PWV map. Credit: NASA/JPL

Lastly, we discuss the errors that arise from our assumption that the temperature of the non-atmospheric region is the same as the air temperature. As noted earlier, by assuming that the air and non-atmospheric surroundings are at the same temperature, we were able to consider the net incoming flux as simply the differential between an ideal blackbody over the full $2\pi$ steradians and the transmissive component of the atmosphere. We used Eqn. 8

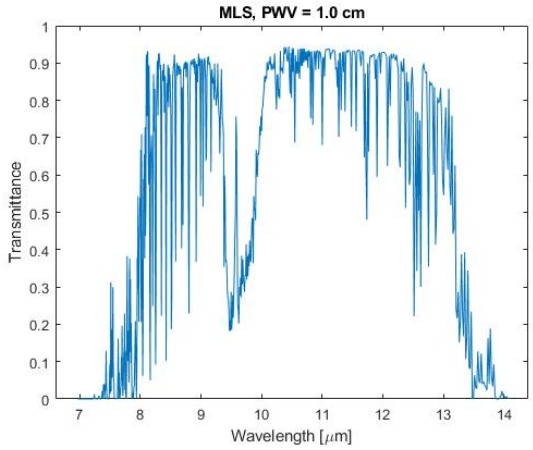


FIG. 5. Sample of wavelength-dependent Modtran® transmittance data for 1cm PWV.

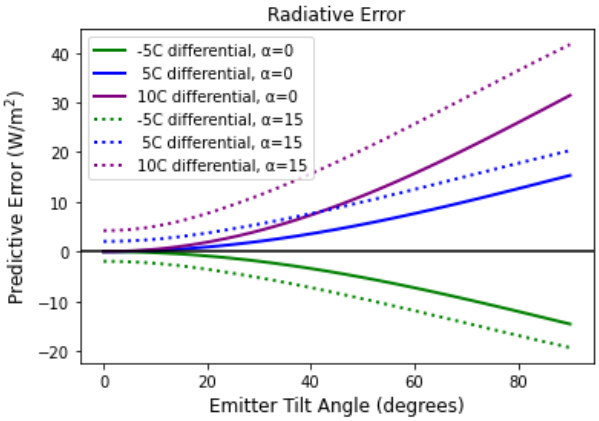


FIG. 6. Curves show the radiative errors arising from the assumption that the air temperature and environmental temperatures are the same. The curves are calculated for an air temperature of 15 °C and environmental temperatures are 10 °C, 20 °C and 25 °C for $\alpha$ being 0°, and 15°. This shows that for emitter tilt angles typically used in dew collection ($\leq 30°$) and above-horizon obstacles limited to a few degrees above horizon, it is a small relative error to assume that the air temperature is the same as the ground temperature even for relatively large temperature differentials. However, significant errors can arise for large obstacle horizon angles and large temperature differentials. Even at a temperature differential of 10 C° and an emitter tilt of 30°, a relative error of 10% to 20% is possible.

in this situation. If the air is not the same temperature, we must calculate the incoming flux from the atmosphere and the non-atmospheric environment separately. We determine the ideal blackbody radiation coming from the solid angle that lies below the obstacle cone

276 impinging on the emitter from

$$p_{env}(T) = (B_1 + B_2) \int_0^\infty I_{BB}(\lambda, T) d\lambda, \tag{20}$$

277 where

$$B_1 = \int_0^\pi \int_{\pi/2-\alpha}^{+\pi/2+\tan^{-1}(\tan(\theta_e)\sin(\phi))} f(\theta_e, \theta, \phi) d\theta d\phi \tag{21}$$

278 and

$$B_2 = \int_0^\pi \int_{\theta_b(\theta_e,\alpha,\phi)}^{-\pi/2+\tan^{-1}(\tan(\theta_e)\sin(\phi))} f(\theta_e, \theta, \phi) d\theta d\phi \tag{22}$$

279 The radiative power errors, in our initial calcuations, arising from having a temperature
280 differential are then given by

$$Error = p_{env}(T_{env}) - p_{env}(T_{air}). \tag{23}$$

281 Consider the results in Fig. 6. The figure assumes that the environmental radiation is
282 still has a uniform, but different temperature from the air. The figure shows the curves for
283 the environment being -5 °C, 5 °C or 10 °C hotter than the air (assumed to be 15 °C) for $\alpha$ of
284 0° and 15°. Comparing Fig. 2 and Fig. 6 at large tilt angles, the relative error can actually
285 produce net positive heating rather than cooling. Owing to the predominant use of emitters
286 at or below angles of 30°, and often in environments with minimal above-horizon obstacles,
287 this figure shows that the assumption that the environment is the same temperature as the
288 air is reasonable, which greatly simplifies the necessary predictive meteo data. However, it
289 does prescribe the need for careful attention to the surroundings when performing radiative
290 cooling. We also see that when the non-atmospheric environment is colder than the air,
291 for example from radiative cooling, it can enhance, as perhaps expected, the cooling of the
292 system. In this case, the radiative error can actually improve the net radiative deficit shown
293 in Fig. 2. This is one of the reasons why emitters that face each other, or have conical
294 geometries, can actually slightly increase yield.

295 ## VII. CONCLUSION

296 In this paper, we have derived a clear sky, radiative theory that accounts for planar emitter
297 tilt, precipitable water vapor and near-horizon obstacles and formulated an extension of the

theory to non-zero cloud cover. We are able to make estimates of the radiative cooling power and thus dew yield given the surface temperature, relative humidity and atmospheric water vapor scale height. This is an important and necessary improvement of the former theories elaborated for horizontal radiative surfaces. We have shown that the error made in assuming the subhorizon temperature equal to air temperature is of the order of a few percent for tilt angles lower than 30°. We believe that a tilt-dependent emitter radiative theory will be beneficial to the understanding of dew collection.


[1] "Modtran," `http://modtran.spectral.com`.

[2] Daniel Beysens, *Dew water* (River Publishers, 2018).

[3] Marlene Tomaszkiewicz, Majdi Abou Najm, Daniel Beysens, Ibrahim Alameddine, and Mutasem El-Fadel, "Dew as a sustainable non-conventional water resource: a critical review," Environmental reviews **23**, 425–442 (2015).

[4] Kudzai F Kaseke and Lixin Wang, "Fog and dew as potable water resources: Maximizing harvesting potential and water quality concerns," GeoHealth **2**, 327–332 (2018).

[5] *Global Risks Report 2019, 14th Edition* (World Economic Forum, 2019).

[6] Mesfin M. Mekonnen and Arjen Y. Hoekstra, "Four billion people facing severe water scarcity," Science Advances **2** (2016), 10.1126/sciadv.1500323, https://advances.sciencemag.org/content/2/2/e1500323.full.pdf.

[7] Taikan Oki and Shinjiro Kanae, "Global hydrological cycles and world water resources," science **313**, 1068–1072 (2006).

[8] V.S. Nikolayev, D. Beysens, A. Gioda, I. Milimouka, E. Katiushin, and J.-P. Morel, "Water recovery from dew," Journal of Hydrology **182**, 19 – 35 (1996).

[9] Marc Muselli, Daniel Beysens, Jacques Marcillat, Irina Milimouk, Torbjorn Nilsson, and Alain Louche, "Dew water collector for potable water in ajaccio(corsica island, france)," Atmospheric Research **64**, 297–312 (2002).

[10] Daniel Beysens, O Clus, Marina Mileta, Iryna Milimouk, Marc Muselli, and VS Nikolayev, "Collecting dew as a water source on small islands: the dew equipment for water project in

bis˘ evo (croatia)," Energy **32**, 1032–1037 (2007).

[11] Girja Sharan, Owen Clus, S Singh, M Muselli, and D Beysens, "A very large dew and rain ridge collector in the kutch area (gujarat, india)," Journal of hydrology **405**, 171–181 (2011).

[12] Girja Sharan, "Harvesting dew with radiation cooled condensers to supplement drinking water supply in semi-arid," International Journal for Service Learning in Engineering, Humanitarian Engineering and Social Entrepreneurship **6**, 130–150 (2011).

[13] B. Khalil, J. Adamowski, A. Shabbir, C. Jang, M. Rojas, K. Reilly, and Bogdan Ozga-Zielinski, "A review: dew water collection from radiative passive collectors to recent developments of active collectors," Sustainable Water Resources Management **2**, 71–86 (2016).

[14] AK Head, "Method and means for refrigeration by selective radiation," Australian Patent (1959).

[15] Raymond W Bliss Jr, "Atmospheric radiation near the surface of the ground: a summary for engineers," Solar Energy **5**, 103–120 (1961).

[16] Torbjörn MJ Nilsson, Gunnar A Niklasson, and Claes G Granqvist, "A solar reflecting material for radiative cooling applications: Zns pigmented polyethylene," Solar Energy materials and Solar cells **28**, 175–193 (1992).

[17] Md. Muntasir Hossain and Min Gu, "Radiative cooling: Principles, progress, and potentials," Advanced Science **3**, 1500360 (2016), https://onlinelibrary.wiley.com/doi/pdf/10.1002/advs.201500360.

[18] Mehdi Zeyghami, D. Yogi Goswami, and Elias Stefanakos, "A review of clear sky radiative cooling developments and applications in renewable power systems and passive building cooling," Solar Energy Materials and Solar Cells **178**, 115 – 128 (2018).

[19] Ming Zhou, Haomin Song, Xingyu Xu, Alireza Shahsafi, Zhenyang Xia, Zhenqiang Ma, Mikhail Kats, Jia Zhu, Boon S Ooi, Qiaoqiang Gan, *et al.*, "Accelerating vapor condensation with daytime radiative cooling," arXiv preprint arXiv:1804.10736 (2018).

[20] Minghao Dong, Zheng Zhang, Yu Shi, Xiaodong Zhao, Shanhui Fan, and Zhen Chen, "Fundamental limits of the dew-harvesting technology," arXiv:1909.05757 (1961).

[21] Bin Zhao, Mingke Hu, Xianze Ao, Nuo Chen, and Gang Pei, "Radiative cooling: A review of fundamentals, materials, applications, and prospects," Applied Energy **236**, 489–513 (2019).

[22] D Beysens, "The formation of dew," Atmospheric research **39**, 215–237 (1995).

[23] Ninari Agam and Pedro R Berliner, "Dew formation and water vapor adsorption in semi-arid environments—a review," Journal of Arid Environments **65**, 572–590 (2006).

[24] Daniel Beysens, Irina Milimouk, Vadim Nikolayev, Marc Muselli, and Jacques Marcillat, "Using radiative cooling to condense atmospheric vapor: a study to improve water yield," Journal of Hydrology **276**, 1–11 (2003).

[25] JF Maestre-Valero, V Martinez-Alvarez, A Baille, B Martín-Górriz, and B Gallego-Elvira, "Comparative analysis of two polyethylene foil materials for dew harvesting in a semi-arid climate," Journal of hydrology **410**, 84–91 (2011).

[26] J.F. Maestre-Valero, R. Ragab, V. MartÃnez-Alvarez, and A. Baille, "Estimation of dew yield from radiative condensers by means of an energy balance model," Journal of Hydrology **460-461**, 103 – 109 (2012).

[27] Zhen Chen, Linxiao Zhu, Aaswath Raman, and Shanhui Fan, "Radiative cooling to deep sub-freezing temperatures through a 24-h day–night cycle," Nature communications **7**, 13729 (2016).

[28] Yao Zhai, Yaoguang Ma, Sabrina N. David, Dongliang Zhao, Runnan Lou, Gang Tan, Ronggui Yang, and Xiaobo Yin, "Scalable-manufactured randomized glass-polymer hybrid metamaterial for daytime radiative cooling," Science **355**, 1062–1066 (2017), http://science.sciencemag.org/content/355/6329/1062.full.pdf.

[29] Pierre-Brice Bintein, Henri Lhuissier, Anne Mongruel, Laurent Royon, and Daniel Beysens, "Grooves accelerate dew shedding," Physical review letters **122**, 098005 (2019).

[30] Hua Bao, Chen Yan, Boxiang Wang, Xing Fang, C.Y. Zhao, and Xiulin Ruan, "Double-layer nanoparticle-based coatings for efficient terrestrial radiative cooling," Solar Energy Materials and Solar Cells **168**, 78–84 (2017).

[31] Huade Guan, Megan Sebben, and John Bennett, "Radiative- and artificial-cooling enhanced dew collection in a coastal area of south australia," Urban Water Journal **11**, 175–184 (2013).

[32] Omar Al-Khayat, Jun Ki Hong, David M. Beck, Andrew I. Minett, and Chiara Neto, "Patterned polymer coatings increase the efficiency of dew harvesting," ACS Applied Materials & Interfaces **9**, 13676–13684 (2017).

[33] Owen Clus, Pascal Ortega, Marc Muselli, Iryna Milimouk, and Daniel Beysens, "Study of dew water collection in humid tropical islands," Journal of Hydrology **361**, 159–171 (2008).

[34] Marc Muselli, Daniel Beysens, Marina Mileta, and Iryna Milimouk, "Dew and rain water collection in the dalmatian coast, croatia," Atmospheric Research **92**, 455–463 (2009).

[35] Giora J. Kidron, "Angle and aspect dependent dew and fog precipitation in the negev desert," Journal of Hydrology **301**, 66–74 (2005).

[36] A.F.G. Jacobs, B.G. Heusinkveld, and S.M. Berkowicz, "Passive dew collection in a grassland area, the netherlands," Atmospheric Research **87**, 377 – 385 (2008), third International Conference on Fog, Fog Collection and Dew.

[37] R Ziatdinov, R Nabiyev, H s Kim, and S H Lim, "The concept of a dew collection device based on the mathematical model of sliding liquid drops on an inclined solid surface," IOP Conference Series: Earth and Environmental Science **272**, 022091 (2019).

[38] D. Beysens, F. Broggini, I. Milimouk-Melnytchouk, J. Ouazzani, and N. Tixier, "New architectural forms to enhance dew collection," Chemical Engineering Transactions **34**, 79–84 (2013).

[39] Benz Kotzen, "Innovation and evolution of forms and materials for maximising dew collection," Ecocycles **1**, 39–50 (2015).

[40] Daniel Beysens, Robert Cooke, Enrico Crobu, and Laurent Royon, "Computational fluid dynamics study of a corrugated hollow cone for enhanced dew yield," Journal of Hydrology **592**, 125788 (2021).

[41] Danilo Carvajal, Jean-Gabriel Minonzio, Elvira Casanga, Jorge Muñoz, Alvaro Aracena, Sonia Montecinos, and Daniel Beysens, "Roof-integrated dew water harvesting in combarbalá, chile," Journal of Water Supply: Research and Technology - Aqua **67**, 357–374 (2018).

[42] Girja Sharan, Anil Kumar Roy, Laurent Royon, Anne Mongruel, and Daniel Beysens, "Dew plant for bottling water," Journal of Cleaner Production **155**, 83–92 (2017).

[43] CG Granqvist and A Hjortsberg, "Radiative cooling to low temperatures: General considerations and application to selectively emitting sio films," Journal of Applied Physics **52**, 4205–4220 (1981).

[44] Paul Berdahl and Richard Fromberg, "The thermal radiance of clear skies," Solar Energy **29**, 299–314 (1982).

[45] Dongliang Zhao, Ablimit Aili, Yao Zhai, Jiatao Lu, Dillon Kidd, Gang Tan, Xiaobo Yin, and Ronggui Yang, "Subambient cooling of water: Toward real-world applications of daytime radiative cooling," Joule **3**, 111–123 (2019).

[46] D. Beysens, "Estimating dew yield worldwide from a few meteo data," Atmospheric Research **167**, 146 – 155 (2016).

[47] Cossi Norbert Awanou, "Clear sky emissivity as a function of the zenith direction," Renewable Energy **13**, 227–248 (1998).

[48] Joseph A Shaw and Paul W Nugent, "Physics principles in radiometric infrared imaging of clouds in the atmosphere," European Journal of Physics **34**, S111 (2013).

[49] G. P. Anderson, S. A. Clough, F. X. Kneizys, J. H. Chetwynd, and E. P. Shettle, *AFGL atmospheric constituent profiles (0 - 120 km)*, Tech. Rep. (1986).